Wavefield tomography

Velocity model building remains one of the most important, but also one of the most challenging problems in seismic exploration. Accurate imaging in areas characterized by complex geology requires the construction of an accurate and high resolution velocity model. Furthermore, it is helpful if the velocity model used for wavefield migration, e.g. by reverse-time migration, is also constructed using a wavefield-based technique. In this paper, we use the terminology *wavefield tomography* to describe any method for velocity model building which is based on band-limited wave propagation.

The seismic exploration literature features many wavefield tomography techniques. Generally speaking, these techniques can be classified by the domain in which the optimization problem is formulated. Thus, we can describe wavefield tomography in the data domain or in the image domain. However, the essential component of all methods is the seismic wavefield reconstruction in the subsurface using a numeric solution to a wave-equation, usually the acoustic wave-equation. The essential difference between the data-domain and image-domain techniques is the objective function used to formulate the problem and not the fact that we use the full wavefield for optimization, which is a common feature. In this paper, we restrict our attention to an image-domain technique based on the analysis of semblance between migrated images for overlapping experiments.

Extended imaging condition

Conventional seismic imaging methods share the assumption of single scattering at discontinuities in the subsurface. Under this assumption, waves propagate from seismic sources, interact with discontinuities and return to the surface as reflected seismic waves. The two wavefields kinematically coincide at discontinuities of material properties in the subsurface. The problem is that we do not know a-priori where such discontinuities exist. Therefore, in general we cannot use the difference between the source and receiver wavefields to construct an objective function for velocity optimization. In this case, we need to exploit the principle of invariance of images constructed by different seismic experiments (i.e. the *semblance principle*).

The image, which is the reflectivity information, can be extracted from the reconstructed wavefields by the application of an extended imaging condition:

$$R\left(\mathbf{x},\boldsymbol{\lambda},\tau\right)=\sum_{shots}\sum_{\omega}\overline{W_s\left(\mathbf{x}-\boldsymbol{\lambda},\omega\right)}W_r\left(\mathbf{x}+\boldsymbol{\lambda},\omega\right)e^{2i\omega\tau}\ . \tag{1}$$

The image R is a function of the space coordinates $\mathbf{x}$, and of the space- and time-lag extensions, $\boldsymbol{\lambda}$ and τ (Rickett and Sava, 2002; Sava and Fomel, 2006). For correct velocity, events corresponding to all experiments focus at zero space- and time-lags, Figures 1(a)-1(d) (Sava and Vasconcelos, 2009).

Semblance analysis

As discussed by Sava and Vasconcelos (2009), extensions can be analyzed effectively in common-image-point-gathers constructed at some locations in the image. In this way, we achieve several objectives: (1) we sample the image more-or-less densely, depending on the structure itself, (2) we do not construct extensions at every grid point along the vertical axis, (3) we do not compute extensions at locations in the image that are not appropriate for MVA, and (4) we do not bias our analysis toward nearly-horizontal events. Such CIPs are the natural companions to RTM which is also not biased toward a specific extrapolation axis. Furthermore, the extended images can be decomposed as a function of incidence angles at the reflector (Sava and Fomel, 2003). As discussed earlier, the MVA optimization problem is based on the semblance principle which uses the fact that the Earth reflectivity is invariant relative to the seismic experiment used for imaging. This process can be implemented by measuring flatness in the angle-domain or by measuring focusing in the space-lag/time-lag domain, i.e. we can analyze the focusing of CIP gathers at fixed locations in the image, $R\left(\boldsymbol{\lambda},\tau\right)$.

We can exploit the extended imaging condition for wavefield tomography using *wave-equation migration velocity analysis* (Biondi and Sava, 1999; Sava and Biondi, 2004; Shen et al., 2005; Albertin et al., 2006; Soubaras and Gratacos, 2007; Symes, 2009). In this technique, we update the velocity

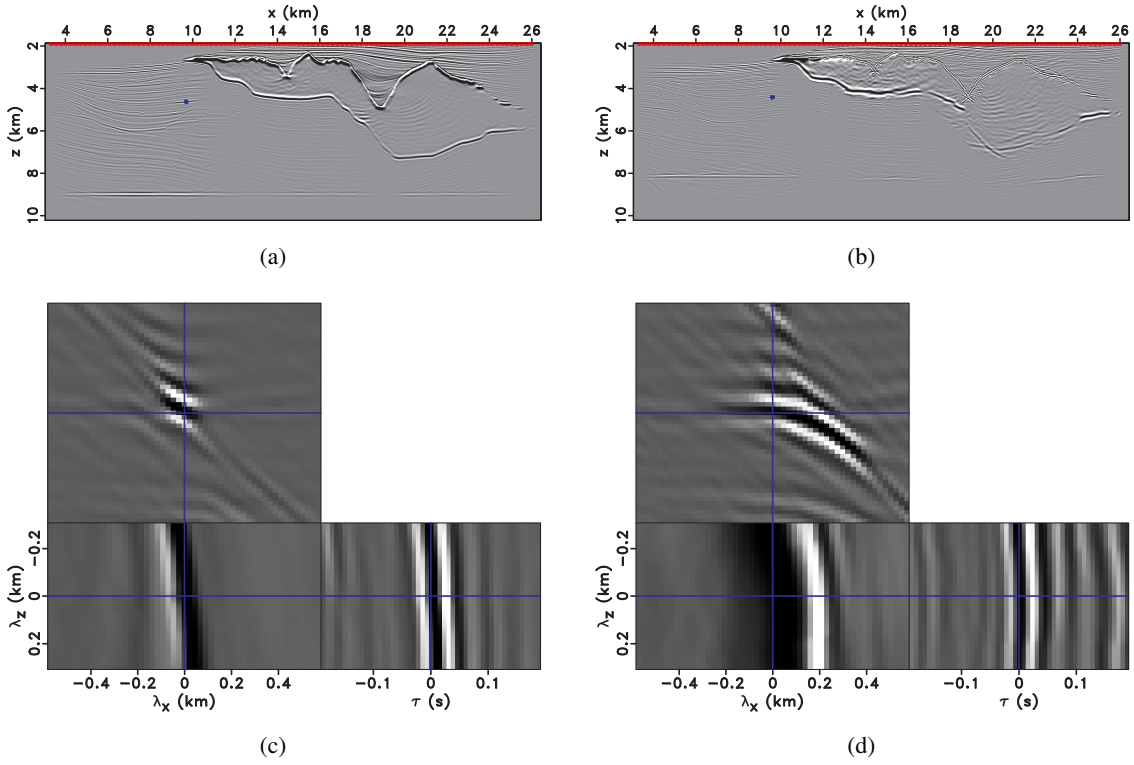


Figure 1: Sigsbee 2A example with migrated images obtained with (a) correct and (b) low velocities. Common-image-point gathers constructed using the extended imaging condition at the locations indicated in the migrated images for (c) correct and (d) low velocities.

model by constructing an objective function that penalizes the departure of the migrated image from an ideal shape, i.e. by minimizing the objective function

$$J(v) = \sum_{\mathbf{x}} \sum_{\boldsymbol{\lambda},\tau} \frac{1}{2} \| \mathbf{P}_{\{\boldsymbol{\lambda},\tau\}} \left[R(\mathbf{x}, \boldsymbol{\lambda}, \tau) \right] \|^2 . \tag{2}$$

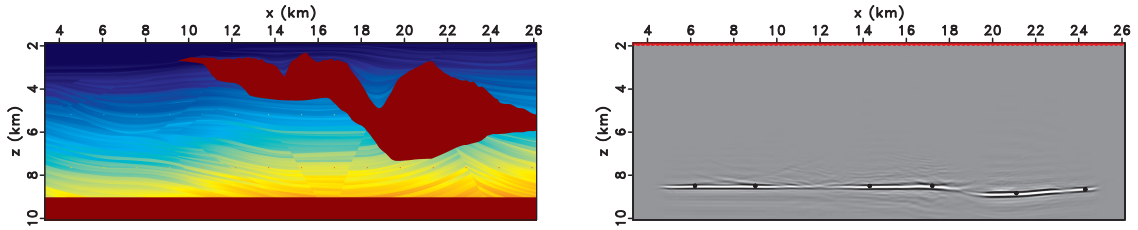
In this expression, $\mathbf{P}$ is a penalty operator which depends on the space- and time-lag variables, $\boldsymbol{\lambda}$ and τ. We do not need to assume that we know the source function, but we assume that the source is invariant from one experiment to another. An optimal penalty operator $\mathbf{P}$ uses the differential semblance principle (Symes and Carazzone, 1991) leading to a objective function which is smooth and uni-modal, thus facilitating gradient-based optimization. Figures 3(a)-3(f) show two options for applying the differential semblance process to the extended images. Panels (a)-(c) correspond to DSO applied to CIGs constructed at fixed surface positions (Shen and Symes, 2008), while panels (d)-(f) correspond to DSO applied to CIPs constructed at fixed image positions. The penalty functions have similar features, i.e. higher penalty applies to the image components that depart from the ideal image location at $\lambda_x = 0$, or at $\{\boldsymbol{\lambda} = 0, \tau = 0\}$, respectively.

Sensitivity kernels

The application of a penalty operator $\mathbf{P}$ to an extended image R produces an image perturbation, as discussed by Sava and Biondi (2004) for space-lag extensions or by Yang and Sava (2009) for time-lag extensions. Wave-equation migration velocity analysis converts this image perturbation into an update of the slowness model by the application of a linear operator $\mathbf{L}$ based on the band-limited wavefield extrapolated in the background slowness model (Sava and Vlad, 2008):

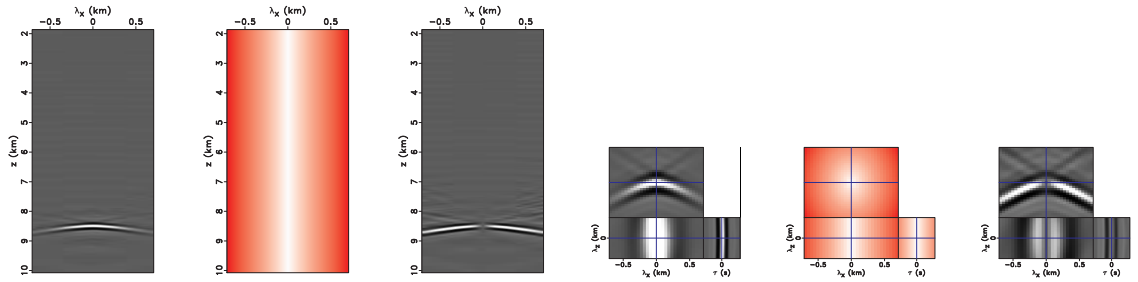
$$\Delta R = \mathbf{L} \Delta s \ , \tag{3}$$

where $\Delta R = \mathbf{P}_{\{\boldsymbol{\lambda},\tau\}} \left[R(\mathbf{x}, \boldsymbol{\lambda}, \tau) \right]$. An effective way to study the wave-equation MVA operator $\mathbf{L}$ is through sensitivity kernels. The main elements that control the shape of the sensitivity kernels are (1)



(a) (b)

Figure 2: Synthetic example using (a) the Sigsbee velocity model and one horizontal reflector at 9 km in depth. Panel (b) is the image obtained with an incorrect (low) velocity. The dots overlain on the figure indicate the locations where CIPs are constructed.



(a) (b) (c) (d) (e) (f)

Figure 3: Extended images constructed at the locations indicated by the dots in Figure 2(b). Panels (a)-(c) correspond to CIGs and panels (d)-(f) correspond to CIPs. Panels (b) and (e) depict the penalty functions applied to the images shown in panels (a) and (d), respectively. Panels (c) and (f) depict the penalized extended images used in the objective function given by equation 2.

the frequency content of the background wavefield, (2) the type of source from which we generate the background wavefield, and (3) the type of perturbation introduced in the image space.

Figures 4(a)-4(d) show sensitivity kernels for the model shown in Figure 2(a). All kernels correspond to wavefields constructed in the same frequency band and with many point sources located on the surface. Panels (a) and (b) represent sensitivity kernels for one CIG or CIP, respectively. Panels (c) and (d) represent the superposition of kernels for 6 CIGs or CIPs, respectively. In all cases, we observe that the kernels constructed using CIGs and CIPs are similar, indicating that the CIP procedure is effective and comparable to the more conventional procedure using CIGs. At the same time, DSO using CIPs is a more computationally effective procedure, because the extensions need not be computed at all locations in the image, but can follow the geologic structure, as discussed earlier. Finally, we note that in more complex geologic settings, the penalty function discussed earlier needs to be modified in order to avoid interference between close events.

Conclusions

Wavefield tomography can be formulated based on extended imaging conditions. In particular, we can formulate differential semblance optimization based on extended common-image-point gathers constructed at sparse locations in the image, thus leading to a flexible and robust velocity updating technique. This paper presents just one of many possibilities of penalty functions applicable to extended images. A numeric example demonstrates the feasibility of velocity updating scheme using extended images.

Acknowledgments

This work is supported by the sponsors of the Center for Wave Phenomena at Colorado School of Mines and by a research grant from Statoil.

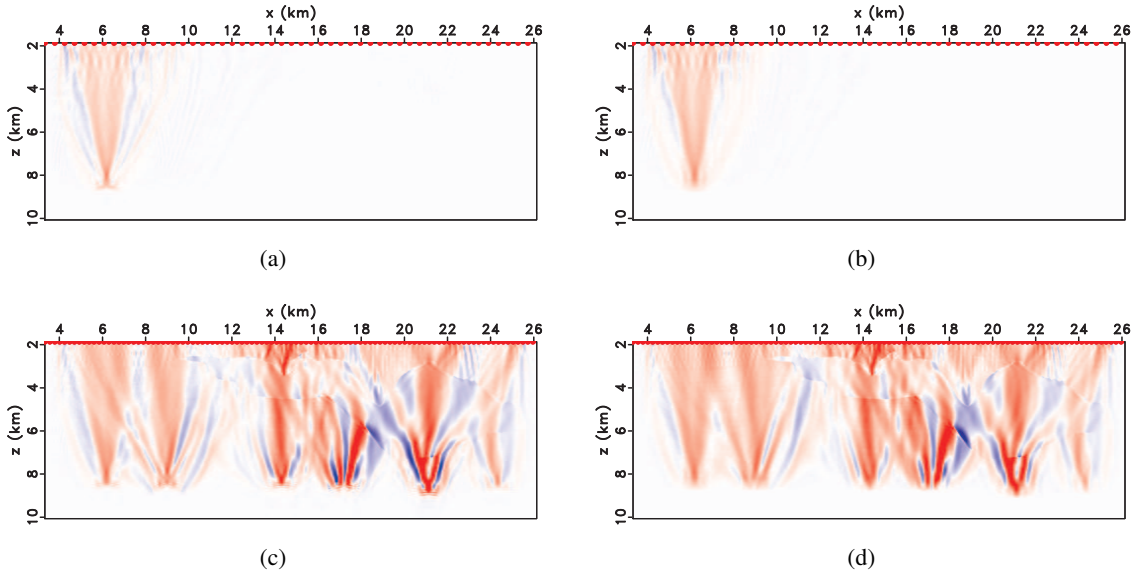


Figure 4: Sensitivity kernels for the model shown in Figure 2(a). Panels (a) and (b) are sensitivity kernels for one CIG and one CIP, respectively. Panels (c) and (d) are sensitivity kernels for all CIGs and all CIPs, respectively.

REFERENCES

Albertin, U., P. Sava, J. Etgen, and M. Maharramov, 2006, Image differencing and focusing in wave-equation velocity analysis: Presented at the 68th Mtg., Abstracts, Eur. Assoc. Expl. Geophys.

Biondi, B., and P. Sava, 1999, Wave-equation migration velocity analysis: 69th Annual International Meeting, SEG, Expanded Abstracts, 1723–1726.

Rickett, J., and P. Sava, 2002, Offset and angle-domain common image-point gathers for shot-profile migration: Geophysics, **67**, 883–889.

Sava, P., and B. Biondi, 2004, Wave-equation migration velocity analysis - I: Theory: Geophysical Prospecting, **52**, 593–606.

Sava, P., and S. Fomel, 2003, Angle-domain common image gathers by wavefield continuation methods: Geophysics, **68**, 1065–1074.

———, 2006, Time-shift imaging condition in seismic migration: Geophysics, **71**, S209–S217.

Sava, P., and I. Vasconcelos, 2009, Efficient computation of extended images by wavefield-based migration: Presented at the 79th Annual International Meeting, SEG, Expanded abstracts.

Sava, P., and I. Vlad, 2008, Numeric implementation of wave-equation migration velocity analysis operators: Geophysics, **73**, VE145–VE159.

Shen, P., W. Symes, S. Morton, and H. Calandra, 2005, Differential semblance velocity analysis via shot profile migration: 74th Annual International Meeting, SEG, Expanded Abstracts, 2249–2253.

Shen, P., and W. W. Symes, 2008, Automatic velocity analysis via shot profile migration: Geophysics, **73**, VE49–VE59.

Soubaras, R., and B. Gratacos, 2007, Velocity model building by semblance maximization of modulated-shot gathers: Geophysics, **72**, U67–U73.

Symes, W., 2009, Migration velocity analysis and waveform inversion: Geophysical Prospecting, **56**, 765–790.

Symes, W. W., and J. J. Carazzone, 1991, Velocity inversion by differential semblance optimization: Geophysics, **56**, 654–663.

Yang, T., and P. Sava, 2009, Wave-equation migration velocity analysis using extended images: Presented at the 79th Annual International Meeting, SEG, Expanded abstracts.